WITHDRAWN: Evaluation of global climate models for the simulation of precipitation based on temporal and spatial assessment metrics in China

Yawen Lei

leiyawen@whu.edu.cn

Wuhan University

Research Article

Keywords: CMIP6 GCMs, China, temporal and spatial metrics, Comprehensive rating metrics

Posted Date: June 16th, 2022

DOI: https://doi.org/10.21203/rs.3.rs-1658240/v1

Additional Declarations: No competing interests reported.

EDITORIAL NOTE:

The full text of this preprint has been withdrawn by the authors while they make corrections to the work. Therefore, the authors do not wish this work to be cited as a reference. Questions should be directed to the corresponding author.

Abstract

Global climate models of Coupled Model Inter-comparison Project 6 (CMIP6) has designed with the Shared Socioeconomic Pathways (SSPs) to project future climate change signal. Performance of 21 global climate models (GCMs) of CMIP6 was evaluated in this study in replicating cma rainfall in China for 1961–2014 period. Taylor diagram, Kolmogorov-Smirnov statistic (KS) and six spatial metrics including Goodman-Kruska's lambda (λ), Cramer's V, Theil U, Fraction skill scores (FSS), SPAtial Efficiency metric (SPAEF) and Kling-Gupta efficiency (KGE) are used for the evaluation. Comprehensive rating metrics (RM) based on six spatial metrics were used for the ranking of the GCMs for the evaluation of annual and seasonal precipitation. The results showed that most GCMs overestimate the annual and seasonal precipitation in the mainland of China. Moreover, some differences are indicated in the ranks of GCMs for different metrics. The overall ranks indicated IPSL-CM6A-LR, EC-Earth3-Veg, EC-Earth3, IPSL-CM6A-LR and EC-Earth3 are most suitable GCMs for simulating annual, spring, summer and fall precipitation in Taylor diagram at the resolution of the observations. FGOALS-g3 is the most skillful in annual and four seasonal except fall precipitation but MPI-ESM1-2-HR for fall precipitation in temporal metric, but BCC-CSM2-MR, GFDL-ESM4, EC-Earth3-Veg, BCC-CSM2-MR, MRI-ESM2-0 are the most suitable GCMs for simulating annual, winter, spring, summer and fall precipitation in comprehensive spatial metrics at the resolution of raw GCMs. For the suitable selection of an ensemble of GCMs to reduce uncertainties in climate projections, the approach proposed in this study can be extended to any number of GCMs and climate variables and applicable to any region.

1 Introduction

In recent years, climate change, a complex and multi-dimensional phenomenon, and its impact on human living environment have become a key research issue (Cameron, 2011; Schlosser & Pfirman, 2012). Precipitation and temperature are often used as the major variables in climate change studies (Sheffield and Wood, 2008). Existing studies have shown that changes in the two variables of precipitation and temperature will cause changes in the frequency and intensity of drought (Qaisrani et al., 2021), flood (C. Wu et al., 2014) disasters, heat wave (Brown, 2020),and low temperature events (Y. Wang et al., 2016). It is generally believed that the sharp rise in temperature during the post-industrial revolution has had a significant impact on the global hydrological cycle (Schlosser & Pfirman, 2012), which in turn affects the human production and living environment. Therefore, it is necessary to study the spatial variables of climate model, such as precipitation and temperature (Das et al., 2015). The prediction of climate change is mostly based on the Global Climate Model (GCM) simulating the large scale process of atmospheric circulation system (Lal et al., 2012). The parameterization of some unknown physical processes (Choi et al., 2017) and the lack of initial conditions (Piao et al., 2021) result in the uncertainty of the models. Therefore, it is important to evaluate uncertainty in different models (Tebaldi & Knutti, 2007).

The Couple Model Inter-comparison phase (CMIP) is based on the model comparison results represented by the mid-19th century atmospheric model comparison project. Under the auspices of the World Climate Research Programme (WCRP), the CMIP is developed to gain a better understanding of the past, present, and future climate change in a multi-model environment (Simpkins, 2017). WCRP CMIP6 is developed on the

basis of CMIP historical simulation, organized by IPCC and composed of a series of GCMs (Eyring et al., 2015). The GCMs is developed based on the CMIP, which is mainly used to simulate and predict climate globally (Knutti et al., 2017; Nguyen et al., 2017). Compared with CMIP5, CMIP6 improves climate sensitivity in Earth models, in addition to increased horizontal and vertical resolution (Wyser et al., 2020), and performs better overall in terms of inter-annual variation (Schlosser & Pfirman, 2012). Currently, the CMIP6 already has over 100 GCMs with different resolutions produced by multiple institutions. In the analysis of climate change and its impact, in order to save human resources, a subset of all patterns are usually selected for analysis (L. Gu et al., 2020; Herger et al., 2018; H. M. Wang et al., 2020).

Some studies try to prove the applicability of variables in GCMs, such as precipitation (H. Gu et al., 2015; McMahon et al., 2015). Applicability is usually verified in four aspects: (1) update, considering only the latest generation of GCM, (2) spatial resolution, high resolution is better than low resolution applicability, (3) effectiveness, considering the performance of different GCM, and (4) representativeness, a combination of variables (e. g. precipitation) within GCM (Feenstra et al., 1998). In the above criteria, the third method is used more, where GCM is sorted and selected according to the performance of its simulated historical climate (Mendlik & Gobiet, 2016).

There are currently some methods used to evaluate the performance of historical data of climate models, such as reliability average integration method (Nychka & Tebaldi, 2003), relative entropy (Shukla et al., 2006), Bayesian method (Tebaldi et al., 2005), probability density function (Perkins et al., 2007), hierarchical ANOVA model (Sansom et al., 2013), clustering method (Knutti et al., 2013), correlation method (Jiang et al., 2015), symmetric uncertainty method (Salman et al., 2018), etc. Johnson & Sharma (2009) evaluated the inter-annual variability of GCM, and Thober & Samaniego (2014) selected indicators of extreme precipitation and extreme temperature for evaluation. Ahmadalipour et al. (2017) incorporated some performance evaluation methods, such as root mean square error, average absolute error, correlation coefficient, and comprehensive scoring index to evaluate the accurate performance of GCM historical data. Some studies evaluate GCM from different time scales, daily scale (Perkins et al., 2007), monthly scale (Srinivasa Raju et al., 2017), seasonal scale (Ahmadalipour et al., 2017), and annual scale (M. et al., 2004). In addition to the time scale, some studies have also performed GCM on the spatial scale, such as the spatial area average (Abbasian et al., 2019; Ahmadalipour et al., 2017) and the performance of GCM on the spatial grid (Srinivasa Raju et al., 2017).

Some scholars (McMahon et al., 2015; Räisänen, 2007) believe that there is no widely accepted time scale standard for GCM evaluation. Gleckler et al. (2008) demonstrated that GCM's assessment based on different time scales such as seasonal precipitation can provide important information for water resources management. McMahon et al. (2015) stated that simulations of GCM on annual timescales can produce long-term mean statistical values better than the daily scale. Srinivasa Raju et al. (2017) and Salman et al. (2018) argument provide more useful information for the GCM evaluation in the region, and GCM selection based on their performance at the grid point cannot guarantee its ability to simulate spatial patterns in the regional climate. Koch et al. (2018) and Demirel et al. (2018) argued that the Climate Model Committee is mostly focused on temporal performance of GCMs, ignoring the evaluation of direct spatial performance. They also emphasized the importance of GCM evaluation using multiple spatial metrics.

Tian et al. (2021) conducted a statistical analysis of precipitation data under different scenarios of CMIP6 in four different directions in China, and found that different models performed differently in different regions. Yang et al. (2021) showed that the results of climate models have different simulation effects for different variables in China. Li et al. (2021) demonstrated that different models in the Yangtze River Basin have different degrees of deviation in precipitation prediction. Some studies (Ahmed et al., 2019; Pour et al., 2018; Salman et al., 2018; Srinivasa Raju et al., 2017) considered performance on the study region evaluating GCM, however, they ignore the ability performance of the GCM spatial pattern.

Accordingly, this study focus on the evaluation of the performance of climate variables of GCMs in historical temporal and spatial assessments. On the premise of this research, the existing research hypothesis is that part of the GCM model set based on the ability to simulate the temporal and spatial model of precipitation can be used in China. The rest of the paper is arranged as follows, Section 2 presents a brief introduction of the study area and datasets, and Section 3 presents the methodology, including the GCM performance assessment metrics and comprehensive rating metrics. Section 4 presents the results, followed by the discussion in Section 5 and conclusion in Section 6.

2 Study Area And Datasets

2.1 Study region and data

This study used a gridded meteorological dataset ($0.5^\circ \times 0.5^\circ$) over China for the period of 1961–2014. This dataset contains four climate variables, including daily precipitation, daily minimum and maximum temperature, which is download from the China Meteorological Data Sharing Service System (http://www.cma.gov.cn/) to represent observed data. This gridded dataset came from 2472 in-situ observation gauge stations across China was interpolated using thin plate spline method of GTOPO30 (Global 30 Arc-Second Elevation) data sampling (Zhang et al., 2015).

The daily maximum and minimum temperature and precipitation in the grid of China were used (see Fig. 1). The resolution of observed data are $0.5^\circ \times 0.5^\circ$, and this data is upscale to the raw resolution of different GCMs for comparison.

2.2 GCM temperature and precipitation data

To evaluate the model data, 21 GCM from CMIP6 (Table 1) extracted from the CMIP6 data center (https://esgf-node.llnl.gov/projects/cmip6/) were used to form a multi-GCM collection, which covers the models developed by different research institutions and is well representative. Select daily precipitation (P) data from 1961–2014.

Table 1
CMIP6 GCMs considered in this study

ID	Model name	Modelling center	Country	Resolution in degree
				lon. × lat.
1	BCC-CSM2-MR	Beijing Climate Center	China	1.125° × 1.1213°
2	FGOALS-g3	Institute of Atmospheric Physics,Chinese Academy of Sciences	China	2° × 2.2785°
3	CanESM5	Canadian Center for Climate Modelling and Analysis	Canada	2.8125° × 2.7893°
4	CNRM-CM6-1	Centre National de Recherches Météorologiques, Centre Européen de Recherche et de Formation Avancée en Calcul Scientifique	France	1.4063° × 1.4004°
5	CNRM-ESM2-1			
6	IPSL-CM6A-LR	Institut Pierre-Simon Laplace	France	2.5° × 1.2676°
7	ACCESS-ESM1-5	Collaboration for Australian Weather and Climate Research	Australian	1.8750° × 1.25°
8	ACCESS-CM2			1.8750° × 1.25°
9	EC-Earth3	EC-EARTH consortium published at Irish Centre for High-End Computing	Netherlands–Ireland	0.7031° × 0.7017°
10	EC-Earth3-Veg			
11	INM-CM4-8	Russian Academy of Sciences, Institute of Numerical Mathematics	Russia	2° × 1.5°
12	INM-CM5-0			
13	MIROC6	Atmosphere and Ocean Research Institute (The University of Tokyo), National Institute for Environmental Studies, and Japan Agency for Marine-Earth Science and Technology	Japan	1.4063° × 1.4004°
14	MIROC-ES2L			2.8125° × 2.7893°
15	MRI-ESM2-0	Meteorological Research Institute	Japan	1.1250° × 1.1213°
16	HadGEM3-GC31-LL	Met Office Hadley Centre	UK	1.8750° × 1.25°
17	UKESM1-0-LL			

ID	Model name	Modelling center	Country	Resolution in degree
				lon. × lat.
18	MPI-ESM1-2-HR	Max Planck Institute for Meteorology	Germany	0.9375° × 0.9349°
19	MPI-ESM1-2-LR			1.875° × 1.8647°
20	NorESM2-MM	Bjerknes Centre for Climate Research, Norwegian Meteorological Institute	Norway	1.25° × 0.9424°
21	GFDL-ESM4	Geophysical Fluid Dynamics Laboratory	USA	1.25° × 1°

3 Methodology

In this study, GCMs for annual and seasonal precipitation were first ranked separately (individual ranking) using six spatial performance measures, lambda, Cramer V, Theil U, FSS, SPAEF, and KGE. And then a comprehensive rating metric (RM) (Jiang et al., 2015) was used to rank the GCMs considering the individual ranks determined corresponding to all above the spatial performance measures. The RM values of GCMs obtained for annual and seasonal precipitation were combined for deriving the overall ranks of GCMs. The procedure used for the ranking is outlined as follows.

1. The observed precipitation data for the period 1961–2014 were remapped to the original grid of the GCM-simulated resolution. The rainfall from raw GCMs were interpolated to the resolution of the observation with inverse distance interpolation.

2. Taylor diagram, Kolmogorov-Smirnov statistic, lambda, Cramer V, Theil U, FSS, SPAEF, and KGE were individually applied to annual and seasonal precipitation for the period 1961–2014.

3. The goodness of fit (GOF) estimated by lambda, Cramer V, Theil U, FSS, SPAEF, and KGE for annual and seasonal precipitation were used to rank the GCMs separately.

4. Comprehensive RMs were used to combine the ranks of GCMs determined by the above spatial performance measures separately for annual and seasonal precipitation.

5. RMs were again used to derive the overall ranks of GCMs considering annual and seasonal precipitation together for the entire study area.

6. The top-ranked GCMs based on their overall ranks in replicating daily annual and seasonal precipitation were identified.

3.1 Taylor diagram

Raw GCMs are downscaled to the same resolution of referenced data. And then we use the method developed by Taylor (Taylor, 2001) to summarize model performance in annual and seasonal precipitation based on Pearson R, the correlation coefficient; Standard deviation; and RMSD, centered root-mean-square difference between the simulated and observed data. The simulated GCM performance better, with higher R, smaller Standard deviation and smaller RMSD.

3.2 Kolmogorov-Smirnov statistic (KS)

The Kolmogorov-Smirnov test (Massey, 1951) is taken as a measure to determine the ability of the GCMs to represent the Probability Density Functions (PDFs) of the observed variables (cma precipitation). The KS measures the maximum vertical distance between the Cumulative Distribution Functions (CDFs) of the GCMs and the observation. Its value ranges between 0 and 1 and value closer to 0 refers to a better agreement between the simulated and observed time-scale precipitation. And the statistic is sensitive to the median, variance and shape of the CDFs and can be expressed as follows:

$$\mathrm{KS} = {}_{x}^{\max}\left\{\left|F^{m}\left(x\right) - F^{o}\left(x\right)\right|\right\}$$

1

Where F^{o} and F^{m} are the CDFs of the observations and GCM simulations, respectively. The empirical CDFs (ECDFs) and boxplots of the model simulations and observations are presented for a better comparison of observations and GCM simulations (see Fig. 3).

3.3 Spatial metrics

Spatial metrics (lambda, Cramer V, Theil U, FSS, SPAEF, and KGE) were individual applied on each year from 1961 to 2014 of mean annual and seasonal precipitation. Later, the GOF values of each year were temporally averaged to obtain a value for the entire study area. The details of the metrics are given below.

3.3.1 Goodman–Kruskal's lambda

Goodman–Kruskal's lambda (λ) is used to measure the nominal or categorical association between categorical maps (Goodman & Kruskal, 1954). The lambda coefficient varies between 0 and 1, where a value closer to 1 refers to a higher similarity between the map of model simulations and that of observations of mean annual and seasonal precipitation. The lambda coefficient was calculated using Eq. (2).

$$\lambda = \frac{\sum_{i=1}^{m} max_{j} c_{ij} - max_{j} \sum_{i=1}^{m} c_{ij}}{N - max_{j} \sum_{i=1}^{m} c_{ij}}$$

2

Where max_{j} is the number of classes (categories) in the observed and simulated maps, c_{ij} is a contingency matrix (describes the relationships between the data classes), i and j are the classes in observed and simulated maps respectively, and m represents the number of classes in the observed and simulated maps.

3.3.2 Cramer's V

Cramer's V statistic is used in assessing spatial agreement between observations and model simulations (Zawadzka et al., 2015). Its value ranges between 0 and 1 and value closer to 1 refers to a better agreement between the simulated and observed maps of the climate variable. Cramer's V was calculated using Eq. (3).

$$\mathrm{V} = \sqrt{\frac{x^2}{N\left(min\left(m,n\right)\right)-1}}$$

3

Here,x^2 is chi-square, N is the grand total of observations, m is the number of rows and n is the number of columns. In this exercise m is number of grids in raw GCMs and $n = 2$ (observed and modelled precipitation).

3.3.3 Theil U

Theil U which uses the concept of redundancy used in information entropy method is usually used to calculate inequality in two variables. The inequality index (U) between cma and GCMs rainfall climatology is calculated using Eq. (4).

$$\mathrm{U} = \frac{\sqrt{\frac{1}{N}\sum_{i=1}^{N}\left({x^m}_i - {x^o}_i\right)^2}}{\sqrt{\frac{1}{N}\sum_{i=1}^{N}\left({x^m}_i\right)^2} + \sqrt{\frac{1}{N}\sum_{i=1}^{N}\left({x^o}_i\right)^2}}$$

4

where ${x^m}_i$ represents GCMs precipitation ${x^o}_i$ represents reference precipitation. A zero value of U indicates perfect equality and 1 complete inequality.

3.3.4 Fractions skill score (FSS)

The fractions skill score (Roberts & Lean, 2008) is used for the assessment of spatial agreement between model simulations and observations, FSS value ranges between 0 and 1 where a value closer to 1 refers to a higher agreement between observed and simulated data. Here, FSS between observed (cma) and GCM-simulated data was computed using Eq. (5).

$$\mathrm{FSS} = 1 - \frac{MSE_{(n)}}{MSE_{(n)ref}}$$

5

In Eq. (5) MSE refers mean square error and is calculated using Eqs. (6) and (7).

$$\mathrm{MSE}_{(n)} = \frac{1}{N_x N_y}\sum_{i=1}^{N_x}\sum_{i=1}^{N_y}\left[O_{(n)i,j} - M_{(n)i,j}\right]^2$$

6

$$\mathrm{MSE}_{(n)ref} = \frac{1}{N_x N_y}\left[\sum_{i=1}^{N_x}\sum_{i=1}^{N_y} O^2_{(n)i,j} + \sum_{i=1}^{N_x}\sum_{i=1}^{N_y} M^2_{(n)i,j}\right]$$

7

In Eqs. (6) and (7) N_x and N_y are the number of columns and rows in an observed or simulated map of a climate variable respectively, O and M are observed and simulated data fractions respectively.

3.3.5 SPAtial EFficiency metric (SPAEF)

SPAEF (Demirel et al., 2018) is a robust spatial performance metric which considers three statistical measures, Pearson correlation, coefficient of variation, and histogram overlap, in the assessment of the GOF of a model. SPAEF combines the information derived from the above three independent statistical measures into one metric. The SPAEF values between observed and GCM-simulated data were calculated using Eq. (8). In Eq. (8), α is the Pearson correlation coefficient between observed and GCM-simulated precipitation, β is the spatial variability, and γ is the overlap between the histograms of observed and GCM-simulated precipitation.

$$\mathrm{SPAEF} = 1 - \sqrt{(\alpha-1)^2 + (\beta-1)^2 + (\gamma-1)^2}$$

8

Equations (9) and (10) show the procedure for β and γ calculations respectively. In Eq. (9) σ_m and σ_o refer to standard deviation of GCM-simulated and observed data respectively and μ_m and μ_o refer to the means of GCM-simulated and observed data respectively.

$$\beta = \frac{\left(\frac{\sigma_m}{\mu_m}\right)}{\left(\frac{\sigma_o}{\mu_o}\right)}$$

9

In Eq. (10), K, L, and N refer to histogram values of observations, histogram values of GCM simulations, and the number of bins in a histogram.

$$\gamma = \frac{\sum_{j=1}^{N} min\left(K_j, L_j\right)}{\sum_{j=1}^{N} K_j}$$

10

The SPAEF can have a value between −∞ and 1, where a value closer to 1 indicates higher spatial similarity between the observations and GCM simulations (Koch et al., 2018).

3.3.6 Kling–Gupta efficiency (KGE)

The Kling–Gupta efficiency (Gupta et al., 2009) which considers three statistical measures, (1) Pearson correlation, (2) variability ratio, and (3) bias ratio, in the assessment of model performance is a GOF test developed, for the model performance assessment. In the present study, KGE was calculated between

historical observed data and GCM-simulated data using Eq. (11). KGE values can range between −∞ and 1, where values close to 1 are preferred.

$$\mathrm{KGE} = 1 - \sqrt{(\alpha_P - 1)^2 + (\beta_P - 1)^2 + (\gamma_{RP} - 1)^2}$$

11

In Eq. (11), α_P is the Pearson correlation between observed and GCM-simulated data, β_P is the bias ratio, and γ_{RP} is the variability ratio. Equations (12) and (13) show the calculation of β_P and γ_{RP} respectively.

$$\beta_P = \frac{\mu_m}{\mu_o}$$

12

In Eq. (12), μ_m and μ_o refer to mean of GCM-simulated and observed data respectively.

$$\gamma_{RP} = \frac{CV_m}{CV_o} = \frac{\left(\frac{\sigma_m}{\mu_m}\right)}{\left(\frac{\sigma_o}{\mu_o}\right)}$$

13

In Eq. (13), CV_m and CV_o refer to the coefficient of variation of GCM-simulated and observed data respectively.

3.4 Comprehensive rating metrics

The overall ranks of GCMs based on different GOFs were obtained for each season separately using Eq. (14).

$$\mathrm{RM} = 1 - \frac{1}{nm}\sum_{i=1}^{n} rank_i$$

14

In Eq. (14), n refers to the number of GCMs, m refers to the number of metrics and i refers to the rank of a GCM based on the i-th GOF. A value of RM near to 1 refers to a better GCM in terms of its ability to mimic the spatial and temporal characteristics of observations.

4 Results And Discussion

4.1 Performance of GCMs in Taylor Diagram

Figure 2 illustrates the Taylor diagrams for annual and seasonal precipitation to evaluate the performance of the GCMs that downscaled to the resolution of the reference one relative to the cma observations. The diagram indicates that the correlation of the simulations with observed annual precipitation varies between 0.7 and 0.9, while this correlation is smaller for summer and fall precipitation, larger spread for winter, spring precipitation. According to the Taylor diagram, the IPSL-CM6A-LR, EC-Earth3 can be identified as the two top-

ranked GCMs for annual precipitation; the EC-Earth3-Veg, EC-Earth3 can be identified as the two top-ranked GCMs for winter precipitation; the EC-Earth3, CNRM-ESM2-1 can be identified as the two top-ranked GCMs for spring precipitation; the IPSL-CM6A-LR, EC-Earth3 can be identified as the two top-ranked GCMs for summer precipitation; the EC-Earth3, EC-Earth3-Veg can be identified as the two top-ranked GCMs for fall precipitation.

4.2 Performance of GCMs in KS

Figure 3 illustrates the ECDFs and boxplots for annual and seasonal precipitation to evaluate the performance of the GCMs that we upscale reference data to the resolution of raw GCMs. We can conclude that almost all the annual and seasonal precipitation of GCMs simulations are larger than the observation in time series, especially in annual, winter, and spring precipitation. However, the summer and fall precipitation of the GCMs simulations show closer relative to the cma precipitation. According to the ECDFs and boxplots, the FGOALS-g3, EC-Earth3 can be identified as the two top-ranked GCMs for annual precipitation; the FGOALS-g3, NorESM2-MM can be identified as the two top-ranked GCMs for winter precipitation; the FGOALS-g3, EC-Earth3 can be identified as the two top-ranked GCMs for spring precipitation; the FGOALS-g3, BCC-CSM2-MR can be identified as the two top-ranked GCMs for summer precipitation; the MPI-ESM1-2-HR, MRI-ESM2-0 can be identified as the two top-ranked GCMs for fall precipitation.

4.3 Performance of GCMs in spatial metrics

Table. 2 shows the ranks attained by the Raw GCMs corresponding to different metrics for annual precipitation. For example, BCC-CSM2-MR attained ranks 4, 6, 2, 3, 10, 1 in terms of Lambda, Cramer V, Theil U, FSS, SPAEF, and KGE respectively. INM-CM4-8 secured rank 21 for four metrics (i.e. Lambda, Cramer V, Theil U, KGE). Several GCMs attained the same rank for three metrics (e.g. MIROC6 and MPI-ESM1-2-HR).

Table. 2. GOF values and ranks of GCMs obtained using different spatial metrics for mean annual precipitation. Bold numbers within brackets represent the rank of GCMs

No.	Lambda(rank)	Cramer V(rank)	Theil U(rank)	FSS(rank)	SPAEF(rank)	KGE(rank)
1	0.022(4)	0.183(6)	0.482(2)	0.902(3)	0.602(10)	0.643(1)
2	0.066(1)	0.284(1)	0.821(18)	0.748(21)	0.235(21)	0.212(14)
3	0.021(6)	0.179(7)	0.593(8)	0.884(7)	0.479(20)	0.313(10)
4	0.022(5)	0.194(3)	0.66(13)	0.859(13)	0.542(16)	0.258(12)
5	0.025(2)	0.201(2)	0.657(11)	0.859(14)	0.537(17)	0.248(13)
6	0.023(3)	0.19(5)	0.62(9)	0.863(11)	0.526(19)	0.387(7)
7	0.012(11)	0.173(10)	0.629(10)	0.861(12)	0.531(18)	0.387(8)
8	0.01(12)	0.17(11)	0.749(17)	0.846(16)	0.609(8)	0.019(18)
9	0.009(14)	0.134(19)	0.534(4)	0.904(2)	0.593(11)	0.369(9)
10	0.014(9)	0.137(17)	0.417(1)	0.931(1)	0.632(4)	0.6(2)
11	0.001(21)	0.119(21)	1(21)	0.791(20)	0.639(3)	-0.356(21)
12	0.001(19)	0.135(18)	0.927(20)	0.804(19)	0.663(2)	-0.172(20)
13	0.001(20)	0.141(16)	0.737(16)	0.847(15)	0.665(1)	0.156(16)
14	0.002(18)	0.127(20)	0.837(19)	0.827(18)	0.567(15)	-0.013(19)
15	0.019(7)	0.173(9)	0.504(3)	0.9(4)	0.607(9)	0.594(3)
16	0.007(15)	0.146(13)	0.681(14)	0.867(10)	0.628(5)	0.099(17)
17	0.009(13)	0.163(12)	0.66(12)	0.87(9)	0.623(7)	0.175(15)
18	0.017(8)	0.175(8)	0.585(7)	0.875(8)	0.58(13)	0.467(6)
19	0.014(10)	0.191(4)	0.703(15)	0.843(17)	0.587(12)	0.279(11)
20	0.006(16)	0.145(14)	0.538(5)	0.897(5)	0.626(6)	0.481(4)
21	0.006(17)	0.145(15)	0.538(6)	0.897(6)	0.569(14)	0.481(5)

Table. 3 shows the comprehensive ranks of GCMs for annual and seasonal precipitation. GFDL-ESM4, EC-Earth3-Veg, MRI-ESM2-0 and BCC-CSM2-MR is the most skillful GCMs in reproducing the spatial characteristics of winter, spring, fall, annual and summer precipitation respectively.

Table 3
Ranks of GCMs for annual and seasonal precipitation based on rating metric values

No.	Annual precipitation	Winter precipitation	Spring precipitation	Summer precipitation	Fall precipitation
1	1	13	6	1	3
2	16	7	11	17	16
3	7	11	7	15	10
4	10	5	9	10	11
5	8	9	4	14	14
6	6	8	2	5	18
7	13	3	8	11	17
8	17	18	16	12	6
9	9	15	5	16	7
10	2	4	1	4	2
11	20	20	21	21	21
12	19	21	19	19	19
13	18	12	18	18	15
14	21	16	20	20	20
15	3	6	3	2	1
16	15	17	17	9	13
17	12	14	15	7	9
18	4	10	12	6	5
19	14	19	14	13	12
20	5	2	10	3	4
21	11	1	13	8	8

The spatial patterns of mean annual, winter, spring, summer and fall precipitation simulated by the GCMs ranked 1 and 21 were compared with the spatial pattern of cma precipitation and presented in Fig. 4. In Fig. 4 it was seen that the GCMs that attained rank 1 (the best-performing GCM) showed spatial patterns more or less similar to those of cma mean annual, winter, spring, summer and fall precipitation. On the other hand, GCMs ranked 21 (the worst-performing GCM) showed large differences compared to the spatial patterns of cma mean annual, winter, spring, summer and fall precipitation. Figure 4 clearly shows that GCMs which

attained rank 21 overestimated the mean annual, winter, spring, summer and fall precipitation over a large region in the study area.

5 Conclusion

This study temporally and spatially assessed the accuracy of 21 CMIP6 GCMs in simulating mean annual and seasonal precipitation over the mainland of China for the period 1961–2014. The spatial evaluation is conducted using six state-of-the-art spatial metrics (lambda, Cramer V, Theil U, FSS, SPAEF, and KGE) and combing with comprehensive rating metric to derive the overall ranks of GCMs based on their ranks pertaining to mean annual and seasonal precipitation, while the temporally evaluation is conducted using KS for the GCMs at raw resolution. And the Taylor diagram is used to evaluate the GCMs downscaled the observations. And the conclusions were drawn from this study as follow.

1. The annual and seasonal analysis of the results showed GCMs simulations overestimate the precipitation in the mainland of China, especially for winter, spring and fall precipitation at the resolution of raw GCMs. And this reveal the necessity of bias correction prior to using GCM outputs of precipitation.

2. Ranks of mean annual and seasonal precipitation driven from 21 GCMs in temporal metrics for the period 1961–2014 is different from that in spatial metrics, summer and fall precipitation get the most similar where the model rank 1st in spatial metrics while rank 2nd in temporal metric. Ranks based on the six spatial metrics (lambda, Cramer V, Theil U, FSS, SPAEF, and KGE) were found different to each other during a given season for precipitation. The performance of GCMs in summer precipitation is most similar to the mean annual precipitation in raw GCMs resolution.

3. IPSL-CM6A-LR, EC-Earth3-Veg, EC-Earth3, IPSL-CM6A-LR and EC-Earth3 are most suitable GCMs for simulating annual, spring, summer and fall precipitation in Taylor diagram at the resolution of the observations, while FGOALS-g3 is the most skillful in annual and four seasonal except fall precipitation but MPI-ESM1-2-HR for fall precipitation at the resolution of raw GCMs, respectively. The overall ranks of GCMs based on a comprehensive rating spatial metric revealed that BCC-CSM2-MR, GFDL-ESM4, EC-Earth3-Veg, BCC-CSM2-MR, MRI-ESM2-0 are the most suitable GCMs for simulating annual and seasonal precipitation at the resolution of raw GCMs.

This results can be helpful to choose suitable GCMs for their related applications for climatologists, hydrologists and water resources managers. We rank the GCMs for annual and seasonal precipitation in the mainland of China, the results can also be useful for other locations that have the same physical features (e.g., climate and topography) as the mainland of China.

Declarations

Funding

This work was supported by The National Key Research and Development Program of China(2017YFA0603704) and Natural Science Foundation of Hubei Province of China(2020CFA100).

Conflict of interest

This author declares no competing interests.

Ethics Approval

Not applicable.

Consent to participate

Not applicable.

Consent to publication

Not applicable.

Data availability

The precipitation data of GCMs in CMIP6 is download from https://esgf-node.llnl.gov/search/cmip6/ and of reference is download form http://data.cma.cn/.

Code availability

The SPAEF was calculated with the SPAEF_func.m in matlab. And other spatial metrics can be used in R functions with DescTools package for Goodman-Kruskal's lambda, Cramer's V, Theil U, with verification package for FSS, and with hydroGOF package for KGE. And other custom code was only used for calculations, and it can be provided by contacting the corresponding author.

Author's contribution

YWL conceived the original idea, designed the methodology, and collected the data. YWL performed the simulations. YWL contributed to the interpretation of results. YWL wrote the paper, and YWL revised the paper.

References

1. Abbasian, M., Moghim, S., & Abrishamchi, A. (2019). Performance of the general circulation models in simulating temperature and precipitation over Iran. Theoretical and Applied Climatology, *135*(3–4), 1465–1483. https://doi.org/10.1007/s00704-018-2456-y
2. Ahmadalipour, A., Rana, A., Moradkhani, H., & Sharma, A. (2017). Multi-criteria evaluation of CMIP5 GCMs for climate change impact analysis. Theoretical and Applied Climatology, *128*(1–2), 71–87. https://doi.org/10.1007/s00704-015-1695-4
3. Ahmed, K., Sachindra, D. A., Shahid, S., Demirel, M. C., & Chung, E. S. (2019). Selection of multi-model ensemble of general circulation models for the simulation of precipitation and maximum and minimum temperature based on spatial assessment metrics. Hydrology and Earth System Sciences, *23*(11), 4803–4824. https://doi.org/10.5194/hess-23-4803-2019

4. Barfus, K., & Bernhofer, C. (2015). Assessment of GCM capabilities to simulate tropospheric stability on the Arabian Peninsula. International Journal of Climatology, *35*(7), 1682–1696. https://doi.org/10.1002/joc.4092
5. Brown, S. J. (2020). Future changes in heatwave severity, duration and frequency due to climate change for the most populous cities. Weather and Climate Extremes, *30*, 100278. https://doi.org/10.1016/j.wace.2020.100278
6. Cameron, F. (2011). Guest editorial: Climate change as a complex phenomenon and the problem of cultural governance. *Museum and Society*, *9*(Rosenau 2003), 84–89.
7. Chandler, R. E. (2013). Exploiting strength, discounting weakness: Combining information from multiple climate simulators. *Philosophical Transactions of the Royal Society A: Mathematical, Physical and Engineering Sciences*, *371*(1991). https://doi.org/10.1098/rsta.2012.0388
8. Choi, H. J., Choi, S. J., Koo, M. S., Kim, J. E., Kwon, Y. C., & Hong, S. Y. (2017). Effects of Parameterized Orographic Drag on Weather Forecasting and Simulated Climatology Over East Asia During Boreal Summer. Journal of Geophysical Research: Atmospheres, *122*(20), 10,669 – 10,678. https://doi.org/10.1002/2017JD026696
9. Das, L., Chandra, B., Viswavidyalaya, K., Akhter, J., & Dutta, M. (2015). *Future Monsoon Rain over Gangetic West Bengal Simulated by CMIP5 GCMs*. *April*.
10. Demirel, M. C., Mai, J., Mendiguren, G., Koch, J., Samaniego, L., & Stisen, S. (2018). Combining satellite data and appropriate objective functions for improved spatial pattern performance of a distributed hydrologic model. Hydrology and Earth System Sciences, *22*(2), 1299–1315. https://doi.org/10.5194/hess-22-1299-2018
11. Eyring, V., Bony, S., Meehl, G. A., Ronald, S., & Oceanic, N. (2015). Overview of the Coupled Model Intercomparison Project Phase 6 (CMIP6) experimental design and organisation. Geoscientific Model Development Discussions, *8*(12), 10539–10583. https://doi.org/10.5194/gmdd-8-10539-2015
12. Eyring, V., Bony, S., Meehl, G. A., Senior, C. A., Stevens, B., Stouffer, R. J., & Taylor, K. E. (2016). Overview of the Coupled Model Intercomparison Project Phase 6 (CMIP6) experimental design and organization. Geoscientific Model Development, *9*(5), 1937–1958. https://doi.org/10.5194/gmd-9-1937-2016
13. Feenstra, J. F., Burton, I., Smith, J. B., & Tol, R. S. J. (1998). *Handbook on Methods for Climate Change Impact Assessment and Adaptation Strategies. {V}ersion 2.0*. *May 2014*.
14. Gleckler, P. J., Taylor, K. E., & Doutriaux, C. (2008). Performance metrics for climate models. Journal of Geophysical Research Atmospheres, *113*(6), 1–20. https://doi.org/10.1029/2007JD008972
15. Goodman, L. A., & Kruskal, W. H. (1954). Measures of Association for Cross Classifications*. Journal of the American Statistical Association, *49*(268). https://doi.org/10.1080/01621459.1954.10501231
16. Gu, H., Yu, Z., Wang, J., Wang, G., Yang, T., Ju, Q., Yang, C., Xu, F., & Fan, C. (2015). Assessing CMIP5 general circulation model simulations of precipitation and temperature over China. International Journal of Climatology, *35*(9), 2431–2440. https://doi.org/10.1002/joc.4152
17. Gu, L., Chen, J., Yin, J., C Sullivan, S., Wang, H. M., Guo, S., Zhang, L., & Kim,J. S. (2020). Projected increases in magnitude and socioeconomic exposure of global droughts in 1.5 and 2 °C warmer

climates. *Hydrology and Earth System Sciences*, *24*(1), 451–472. https://doi.org/10.5194/hess-24-451-2020

18. Gupta, H. V., Kling, H., Yilmaz, K. K., & Martinez, G. F. (2009). Decomposition of the mean squared error and NSE performance criteria: Implications for improving hydrological modelling. Journal of Hydrology, *377*(1–2), 80–91. https://doi.org/10.1016/j.jhydrol.2009.08.003
19. Herger, N., Abramowitz, G., Knutti, R., Angélil, O., Lehmann, K., & Sanderson, B. M. (2018). Selecting a climate model subset to optimise key ensemble properties. Earth System Dynamics, *9*(1), 135–151. https://doi.org/10.5194/esd-9-135-2018
20. Iqbal, Z., Shahid, S., Ahmed, K., Ismail, T., Ziarh, G. F., Chung, E. S., & Wang, X. (2021). Evaluation of CMIP6 GCM rainfall in mainland Southeast Asia. Atmospheric Research, *254*(January), 105525. https://doi.org/10.1016/j.atmosres.2021.105525
21. Jiang, Z., Li, W., Xu, J., & Li, L. (2015). Extreme precipitation indices over China in CMIP5 models. Part I: Model evaluation. Journal of Climate, *28*(21), 8603–8619. https://doi.org/10.1175/JCLI-D-15-0099.1
22. Johnson, F., & Sharma, A. (2009). Measurement of GCM skill in predicting variables relevant for hydroclimatological assessments. Journal of Climate, *22*(16), 4373–4382. https://doi.org/10.1175/2009JCLI2681.1
23. Knutti, R., Masson, D., & Gettelman, A. (2013). Climate model genealogy: Generation CMIP5 and how we got there. Geophysical Research Letters, *40*(6), 1194–1199. https://doi.org/10.1002/grl.50256
24. Knutti, R., Rugenstein, M. A. A., & Hegerl, G. C. (2017). Beyond equilibrium climate sensitivity. Nature Geoscience, *10*(10), 727–736. https://doi.org/10.1038/NGEO3017
25. Koch, J., Demirel, M. C., & Stisen, S. (2018). The SPAtial EFficiency metric (SPAEF): Multiple-component evaluation of spatial patterns for optimization of hydrological models. Geoscientific Model Development, *11*(5), 1873–1886. https://doi.org/10.5194/gmd-11-1873-2018
26. Lal, P. N., Mitchell, T., Aldunce, P., Auld, H., Mechler, R., Miyan, A., Romano, L. E., Zakaria, S., Dlugolecki, A., Masumoto, T., Ash, N., Hochrainer, S., Hodgson, R., Islam, T. U., Mc Cormick, S., Neri, C., Pulwarty, R., Rahman, A., Ramalingam, B., … Wilby, R. (2012). National systems for managing the risks from climate extremes and disasters. In *Managing the Risks of Extreme Events and Disasters to Advance Climate Change Adaptation: Special Report of the Intergovernmental Panel on Climate Change* (Vol. 9781107025). https://doi.org/10.1017/CBO9781139177245.009
27. Leung, J. Y. S., Russell, B. D., & Connell, S. D. (2019). Adaptive Responses of Marine Gastropods to Heatwaves. One Earth, *1*(3), 374–381. https://doi.org/10.1016/j.oneear.2019.10.025
28. Li, Y., Yan, D., Peng, H., & Xiao, S. (2021). Evaluation of precipitation in CMIP6 over the Yangtze River Basin. *Atmospheric Research*, *253*(December 2020), 105406. https://doi.org/10.1016/j.atmosres.2020.105406
29. M., M. J., H., S. D. M., N., B. D., S., J. G., J., W. M., & M., C. (2004). Quantification of modelling uncertainties in a large ensemble of climate change simulations. Nature, *430*(August 2004), 768–772. https://doi.org/10.1038/nature02770.1.
30. Massey, F. J. (1951). The Kolmogorov-Smirnov Test for Goodness of Fit. Journal of the American Statistical Association, *46*(253). https://doi.org/10.1080/01621459.1951.10500769

31. McMahon, T. A., Peel, M. C., & Karoly, D. J. (2015). Assessment of precipitation and temperature data from CMIP3 global climate models for hydrologic simulation. Hydrology and Earth System Sciences, *19*(1), 361–377. https://doi.org/10.5194/hess-19-361-2015
32. Mendlik, T., & Gobiet, A. (2016). Selecting climate simulations for impact studies based on multivariate patterns of climate change. Climatic Change, *135*(3–4), 381–393. https://doi.org/10.1007/s10584-015-1582-0
33. Min, S. K., & Hense, A. (2006). A Bayesian approach to climate model evaluation and multi-model averaging with an application to global mean surface temperatures from IPCC AR4 coupled climate models. Geophysical Research Letters, *33*(8), 1–5. https://doi.org/10.1029/2006GL025779
34. Nguyen, H., Mehrotra, R., & Sharma, A. (2017). Can the variability in precipitation simulations across GCMs be reduced through sensible bias correction? Climate Dynamics, *49*(9–10), 3257–3275. https://doi.org/10.1007/s00382-016-3510-z
35. Nychka, D., & Tebaldi, C. (2003). Comments on “calculation of average, uncertainty range and reliability of regional climate changes from AOGCM simulations via the ‘reliability ensemble averaging’ (REA) method.” Journal of Climate, *16*(5), 883–884. https://doi.org/10.1175/1520-0442(2003)016<0883:COCOAU>2.0.CO;2
36. Perkins, S. E., Pitman, A. J., Holbrook, N. J., & McAneney, J. (2007). Evaluation of the AR4 climate models’ simulated daily maximum temperature, minimum temperature, and precipitation over Australia using probability density functions. Journal of Climate, *20*(17), 4356–4376. https://doi.org/10.1175/JCLI4253.1
37. Piao, J., Chen, W., & Chen, S. (2021). Sources of the internal variability-generated uncertainties in the projection of Northeast Asian summer precipitation. Climate Dynamics, *56*(5–6), 1783–1797. https://doi.org/10.1007/s00382-020-05557-z
38. Pour, S. H., Shahid, S., Chung, E. S., & Wang, X. J. (2018). Model output statistics downscaling using support vector machine for the projection of spatial and temporal changes in rainfall of Bangladesh. Atmospheric Research, *213*(June), 149–162. https://doi.org/10.1016/j.atmosres.2018.06.006
39. Qaisrani, Z. N., Nuthammachot, N., Techato, K., & Asadullah. (2021). Drought monitoring based on Standardized Precipitation Index and Standardized Precipitation Evapotranspiration Index in the arid zone of Balochistan province, Pakistan. Arabian Journal of Geosciences, *14*(1). https://doi.org/10.1007/s12517-020-06302-w
40. Räisänen, J. (2007). How reliable are climate models? Tellus, Series A: Dynamic Meteorology and Oceanography, *59*(1), 2–29. https://doi.org/10.1111/j.1600-0870.2006.00211.x
41. Roberts, N. M., & Lean, H. W. (2008). Scale-selective verification of rainfall accumulations from high-resolution forecasts of convective events. Monthly Weather Review, *136*(1), 78–97. https://doi.org/10.1175/2007MWR2123.1
42. Salman, S. A., Shahid, S., Ismail, T., Ahmed, K., & Wang, X. J. (2018). Selection of climate models for projection of spatiotemporal changes in temperature of Iraq with uncertainties. Atmospheric Research, *213*(July), 509–522. https://doi.org/10.1016/j.atmosres.2018.07.008

43. Sansom, P. G., Stephenson, D. B., Ferro, C. A. T., Zappa, G., & Shaffrey, L. (2013). Simple uncertainty frameworks for selecting weighting schemes and interpreting multimodel ensemble climate change experiments. Journal of Climate, *26*(12), 4017–4037. https://doi.org/10.1175/JCLI-D-12-00462.1
44. Schlosser, P., & Pfirman, S. (2012). Earth science for sustainability. Nature Geoscience, *5*(9), 587–588. https://doi.org/10.1038/ngeo1567
45. Shukla, J., DelSole, T., Fennessy, M., Kinter, J., & Paolino, D. (2006). Climate model fidelity and projections of climate change. Geophysical Research Letters, *33*(7). https://doi.org/10.1029/2005GL025579
46. Simpkins, G. (2017). Progress in climate modelling. Nature Climate Change, *7*(10), 684–685. https://doi.org/10.1038/nclimate3398
47. Srinivasa Raju, K., Sonali, P., & Nagesh Kumar, D. (2017). Ranking of CMIP5-based global climate models for India using compromise programming. Theoretical and Applied Climatology, *128*(3–4), 563–574. https://doi.org/10.1007/s00704-015-1721-6
48. Tebaldi, C., & Knutti, R. (2007). The use of the multi-model ensemble in probabilistic climate projections. Philosophical Transactions of the Royal Society A: Mathematical, Physical and Engineering Sciences, *365*(1857), 2053–2075. https://doi.org/10.1098/rsta.2007.2076
49. Tebaldi, C., Smith, R. L., Nychka, D., & Mearns, L. O. (2005). Quantifying uncertainty in projections of regional climate change: A Bayesian approach to the analysis of multimodel ensembles. Journal of Climate, *18*(10), 1524–1540. https://doi.org/10.1175/JCLI3363.1
50. Thober, S., & Samaniego, L. (2014). Robust ensemble selection by multivariate evaluation of extreme precipitation and temperature characteristics. Journal of Geophysical Research, *119*(2), 594–613. https://doi.org/10.1002/2013JD020505
51. Tian, J., Zhang, Z., Ahmed, Z., Zhang, L., Su, B., Tao, H., & Jiang, T. (2021). Projections of precipitation over China based on CMIP6 models. Stochastic Environmental Research and Risk Assessment, *35*(4), 831–848. https://doi.org/10.1007/s00477-020-01948-0
52. Wang, H. M., Chen, J., Xu, C. Y., Zhang, J., & Chen, H. (2020). A Framework to Quantify the Uncertainty Contribution of GCMs Over Multiple Sources in Hydrological Impacts of Climate Change. Earth's Future, *8*(8). https://doi.org/10.1029/2020EF001602
53. Wang, Y., Shi, L., Zanobetti, A., & Schwartz, J. D. (2016). Estimating and projecting the effect of cold waves on mortality in 209 US cities. *Environment International*, *94*(February 2018), 141–149. https://doi.org/10.1016/j.envint.2016.05.008
54. Wu, C., Huang, G., Yu, H., Chen, Z., & Ma, J. (2014). Impact of climate change on reservoir flood control in the upstream area of the Beijiang River basin, South China. Journal of Hydrometeorology, *15*(6), 2203–2218. https://doi.org/10.1175/JHM-D-13-0181.1
55. Wu, Z., Chen, X., Lu, G., Xiao, H., He, H., & Zhang, J. (2017). Regional response of runoff in CMIP5 multi-model climate projections of Jiangsu Province, China. Stochastic Environmental Research and Risk Assessment, *31*(10), 2627–2643. https://doi.org/10.1007/s00477-016-1349-9
56. Wyser, K., Van Noije, T., Yang, S., Von Hardenberg, J., O'Donnell, D., & Döscher, R. (2020). On the increased climate sensitivity in the EC-Earth model from CMIP5 to CMIP6. Geoscientific Model Development, *13*(8), 3465–3474. https://doi.org/10.5194/gmd-13-3465-2020

57. Xuan, W., Ma, C., Kang, L., Gu, H., Pan, S., & Xu, Y. P. (2017). Evaluating historical simulations of CMIP5 GCMs for key climatic variables in Zhejiang Province, China. Theoretical and Applied Climatology, *128*(1–2), 207–222. https://doi.org/10.1007/s00704-015-1704-7
58. Yang, X., Zhou, B., Xu, Y., & Han, Z. (2021). CMIP6 Evaluation and Projection of Temperature and Precipitation over China. Advances in Atmospheric Sciences, *38*(5), 817–830. https://doi.org/10.1007/s00376-021-0351-4
59. You, Q., Cai, Z., Wu, F., Jiang, Z., Pepin, N., & Shen, S. S. P. (2021). Temperature dataset of CMIP6 models over China: evaluation, trend and uncertainty. Climate Dynamics. https://doi.org/10.1007/s00382-021-05691-2
60. Zawadzka, J., Mayr, T., Bellamy, P., & Corstanje, R. (2015). Comparing physiographic maps with different categorisations. Geomorphology, *231*, 94–100. https://doi.org/10.1016/j.geomorph.2014.12.006
61. Zhang, Q., Xiao, M., Singh, V. P., Liu, L., & Xu, C. Y. (2015). Observational evidence of summer precipitation deficit-temperature coupling in China. Journal of Geophysical Research, *120*(19). https://doi.org/10.1002/2015JD023830

Figures

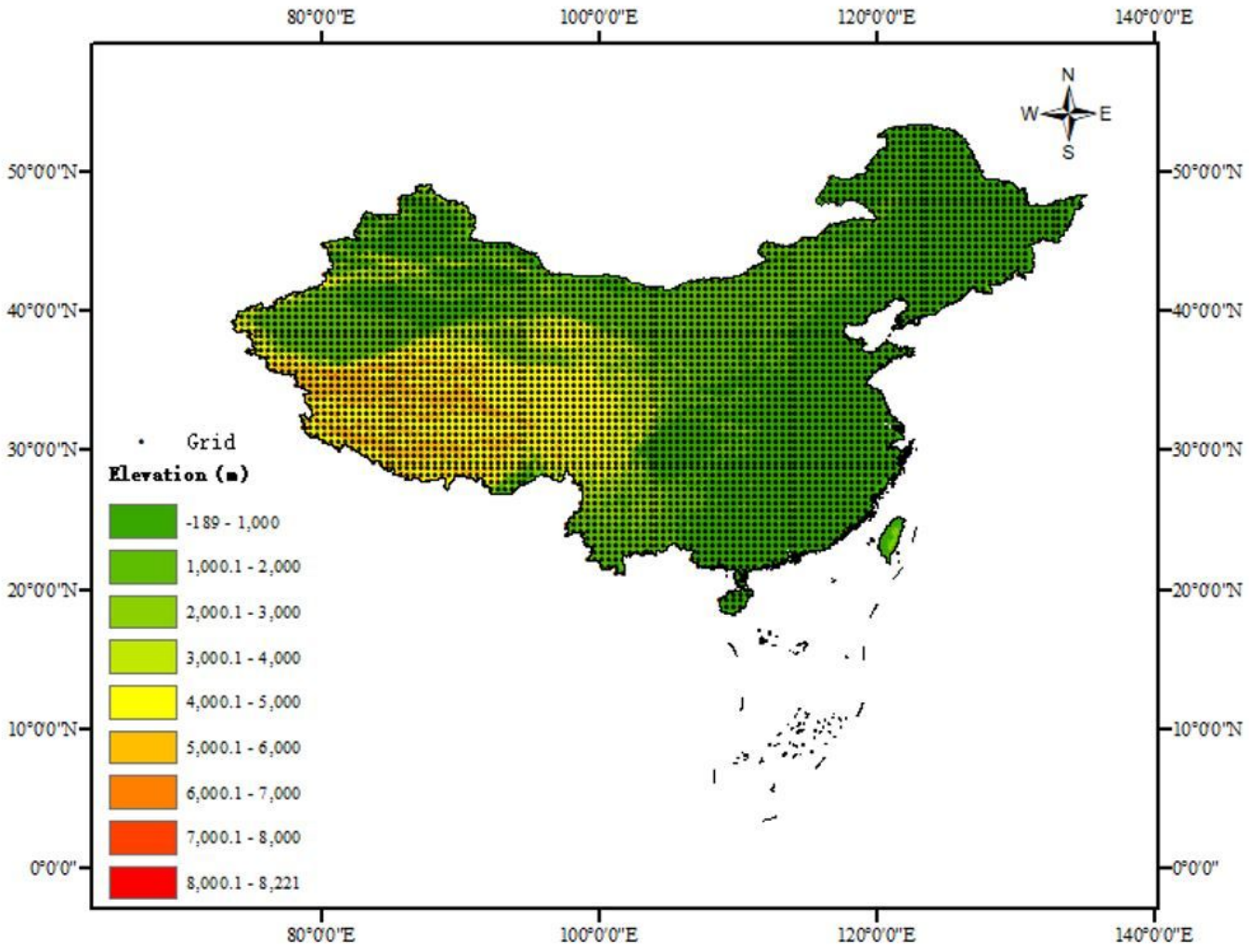

Figure 1

The location of China and the grid points over there.

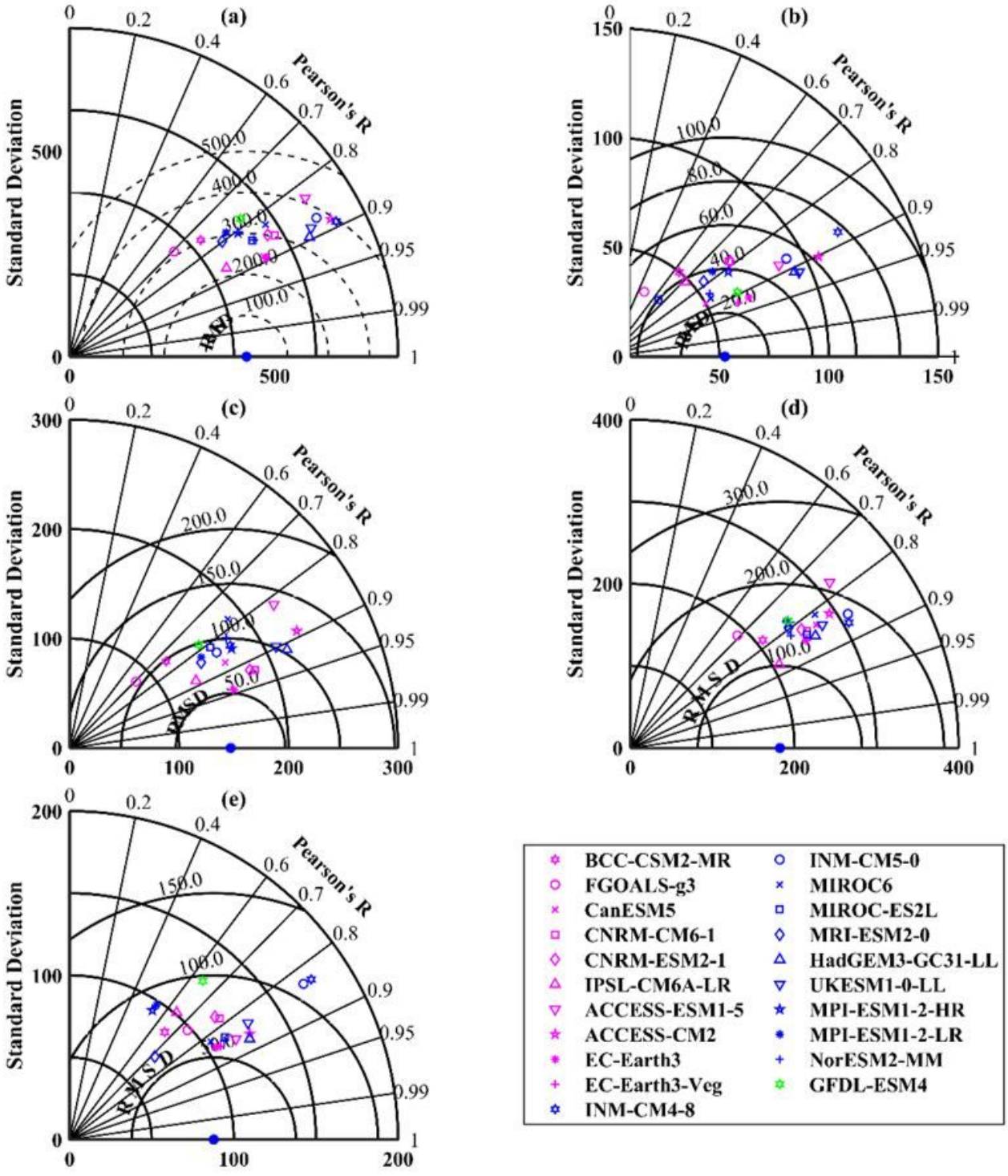

Figure 2

The Taylor diagram of the GCMs simulations for a annual, b winter, c spring, d summer, and e fall precipitation

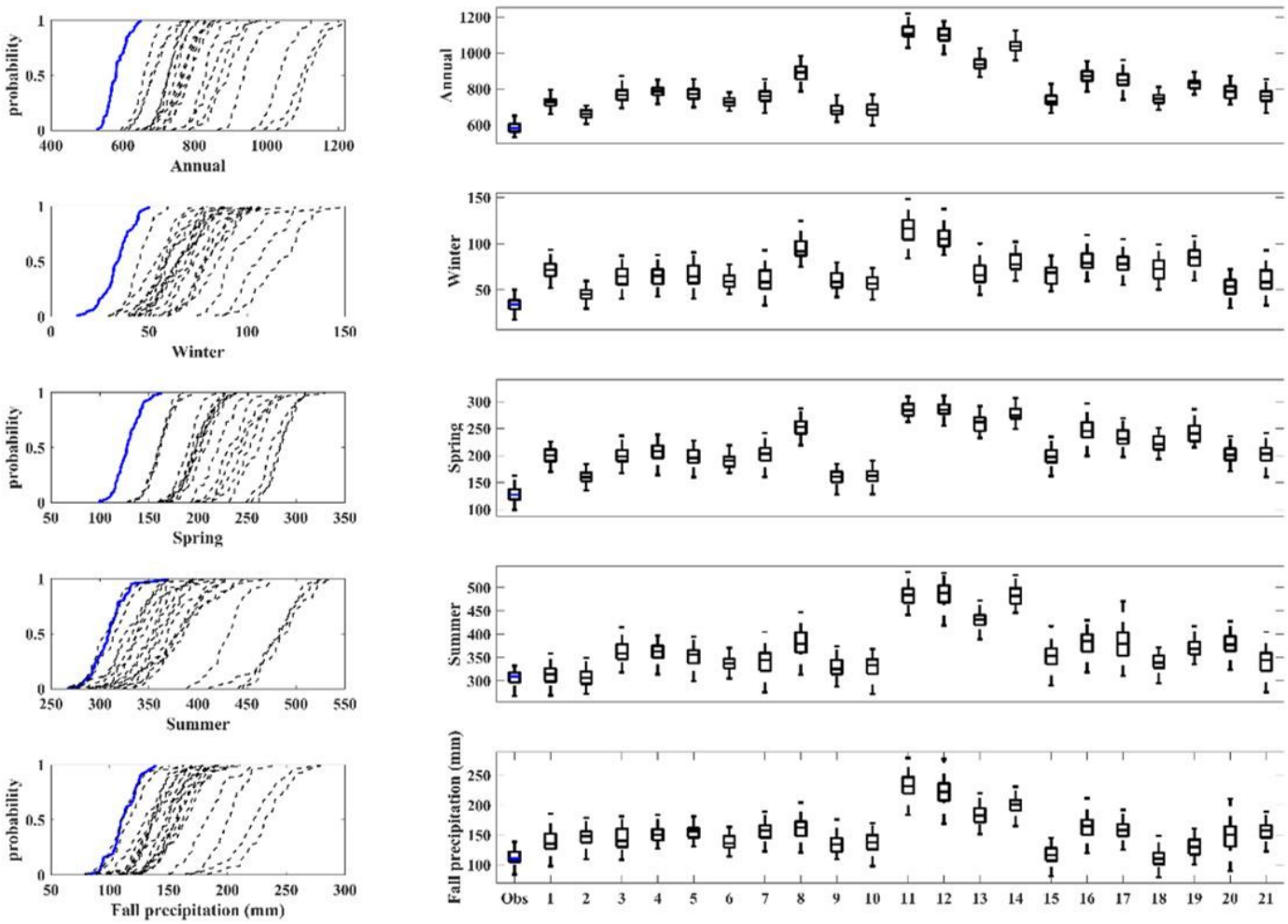

Figure 3

The ECDFs of the cma observations (thick blue lines on the left plots), the ECDFs of the GCM simulations (thin gray lines on the left plots), the bloxplots of the cma observations (blank boxes with blue line on the right plots), and the boxplots of the GCM simulations (blank boxes with black line on the right plots) for annual (first row), winter (second row), spring (third row), summer (fourth row), and fall (fifth row)

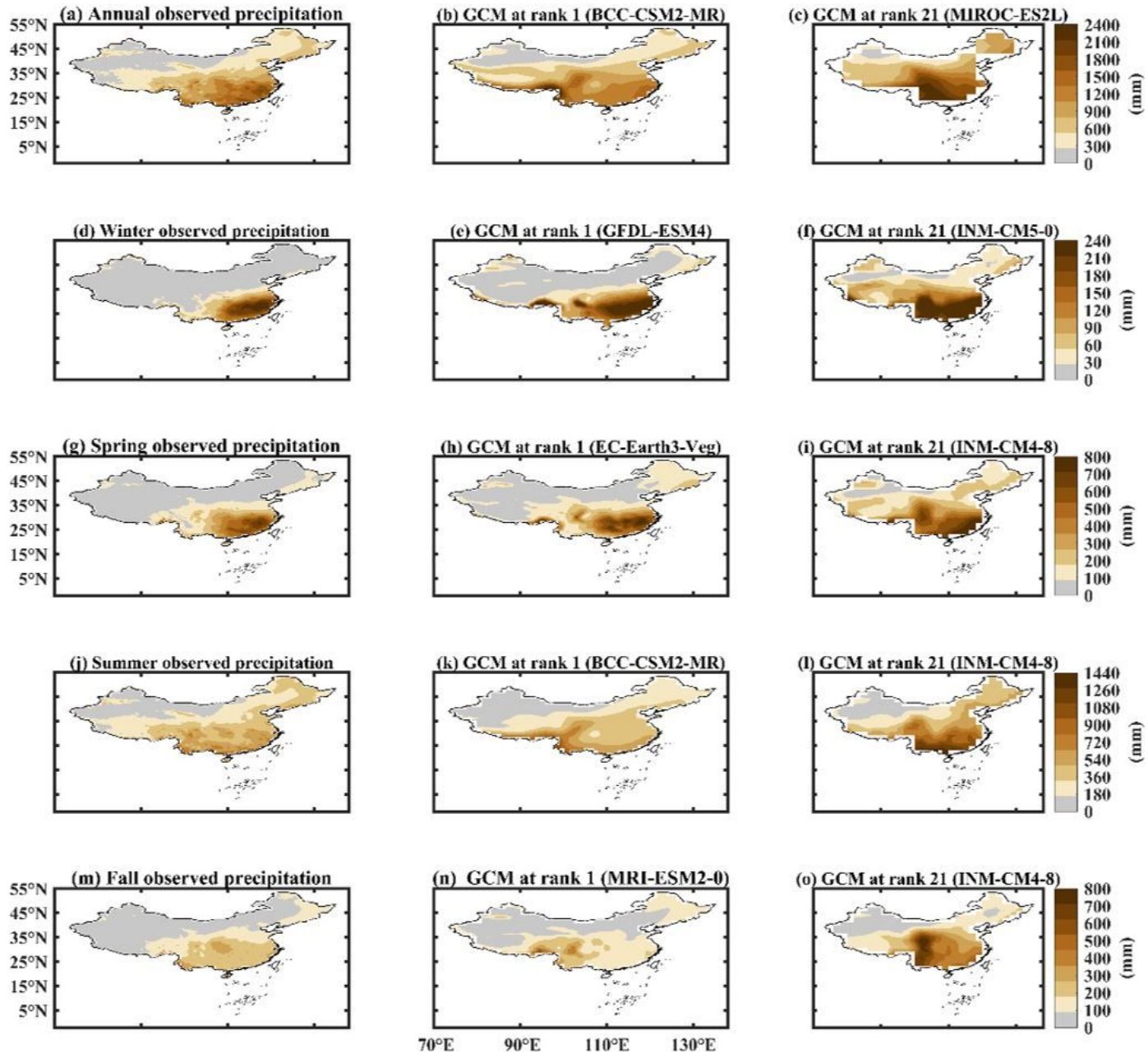

Figure 4

Spatial patterns of cma precipitation (left list), rank 1st precipitation (center list), and ranked 21st precipitation (right list) for annual (first row), winter (second row), spring (third row), summer (fourth row), and fall (fifth row)